PHYSICAL REVIEW A, VOLUME 63, 050703(R)

Angular distribution measurements for spin-orbit-state-resolved S $2p$ photoelectrons of SF_6 in the shape-resonance region

M. Kitajima, M. Hoshino, M. Okamoto, T. Suzuki, and H. Tanaka
Department of Physics, Sophia University, Tokyo 102-8554, Japan

Y. Shimizu,* Y. Muramatsu, H. Chiba, and K. Ueda
Research Institute for Scientific Measurements, Tohoku University, Sendai 980-8577, Japan

T. Hayaishi
Institute of Applied Physics, University of Tsukuba, Tsukuba 305-8577, Japan

M. Simon
LURE, Batiment 209d, Université Paris–Sud, 91405 Orsay Cedex, France
and CEA/DRECAM/SPAM and Laboratoire Francis Perrin, CEN Saclay, 91191 Gif/Yvette Cedex, France

M. Kimura
Graduate School of Science and Engineering, Yamaguchi University, Ube 755-8611, Japan
(Received 13 December 2000; published 17 April 2001)

The angular distributions of the spin-orbit state resolved S $2p$ photoelectrons of SF_6 have been measured in the vicinity of the shape resonances. Relative partial photoionization cross sections of SF_6 into the $(S\ 2p_{3/2})^{-1}$ and $(S\ 2p_{1/2})^{-1}$ states, and the asymmetry parameters of the S $2p_{3/2}$ and S $2p_{1/2}$ photoelectrons are presented. Enhancement of the photoionization cross section into the $(S\ 2p_{3/2})^{-1}$ state at the $(S\ 2p_{1/2})^{-1}\ 2t_{2g}$ resonance has been observed. The excitation photon energy dependence of the asymmetry parameter shows a broad dip at about the photon energies of the resonances. Continuum multiple-scattering calculation of the asymmetry parameters for the $(S\ 2p_{3/2})^{-1}$ and $(S\ 2p_{1/2})^{-1}$ states of SF_6 reproduces this behavior.

DOI: 10.1103/PhysRevA.63.050703 PACS number(s): 33.80.−b, 33.60.−q

It is well known that the inner-shell excitation spectra of ''cage molecules'' containing highly electronegative ligands show ''anomalous'' intensity distributions. A sulfur hexafluoride molecule SF_6 is one of the typical cage molecules and indeed inner-shell excitation spectra of SF_6 that has been studied intensively [1–10]. The anomalous intensity distribution of cage molecules is explained within the potential barrier model in which the cage of electronegative F atoms forms a potential barrier and the excitation of an inner-shell electron into unoccupied molecular orbitals localized inside the potential barrier exhibits anomalously strong resonance features in the inner-shell excitation spectrum [11]. The centrifugal contribution to the potential energy may be combined with electrostatic contributions to produce a potential barrier. Another description for the distinct resonance has been presented without a potential barrier model, in which the origin of the resonance is attributed to the scattering at the steep change of the attractive potential of surrounding atoms [12].

This paper presents the angular distribution measurement of S $2p_{3/2}$ and S $2p_{1/2}$ photoelectrons in the photoionization of SF_6 in the vicinity of the shape resonances. Two strong resonances are observed above the S $2p$ ionization threshold and are assigned as the $(S\ 2p_{3/2,1/2})^{-1}\ 2t_{2g}$ and $(S\ 2p_{3/2,1/2})^{-1}\ 4e_g$ states. Recent high-resolution photoabsorption measurements have shown a splitting of the spin-orbit components of the $(S\ 2p_{3/2,1/2})^{-1}\ 2t_{2g}$ resonance [8]. In the present measurement we resolve the spin-orbit components of S $2p$ photoelectrons and investigate how these spin-orbit components behave in the shape resonance region.

The experiment was carried out using monochromatized synchrotron radiation from a 24-m spherical grating monochromator installed in a beamline 3B at the Photon Factory in Japan [13]. The experimental apparatus has been described in detail elsewhere [14]. Briefly, the incident photon beam was focused onto the interaction region, where the incident photon beam was merged with an effusive gas beam ejected from an axial cell through eight straight needles of 0.5-mm inner diameter. The photoelectrons were energy analyzed by a 150° spherical sector analyzer with a mean radius of 80 mm, which was mounted on a turntable whose axis of rotation was aligned to coincide with the incident photon axis. The incident photon flux was monitored with an Au photocathode mounted behind the interaction region.

The intensity of the photoelectrons ejected at an angle θ with respect to the major axis of the incident photon polarization is given by the following expression:

$$\frac{d\sigma}{d\Omega} = \frac{\sigma}{4\pi}\left\{1+\frac{\beta}{4}(3P\cos 2\theta+1)\right\}, \tag{1}$$

where $d\sigma/d\Omega$ and σ are the differential and partial cross sections for a given ionization process, respectively, β is the asymmetry parameter, and P is the degree of the polarization

*Present address: Institute for Molecular Science, Okazaki 444-8585, Japan.

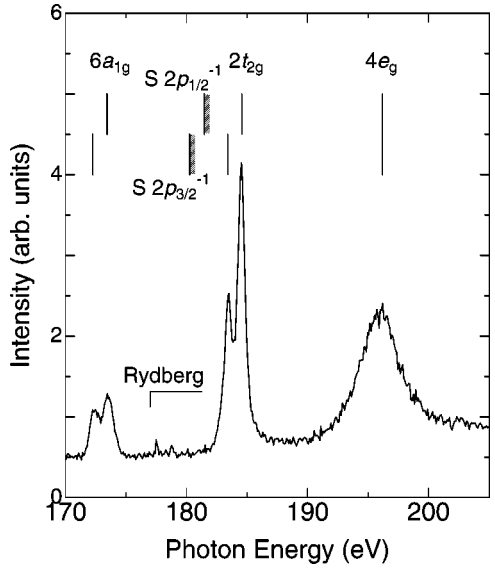

FIG. 1. Total photoion yield spectra of SF_6 near the S $2p$ ionization threshold.

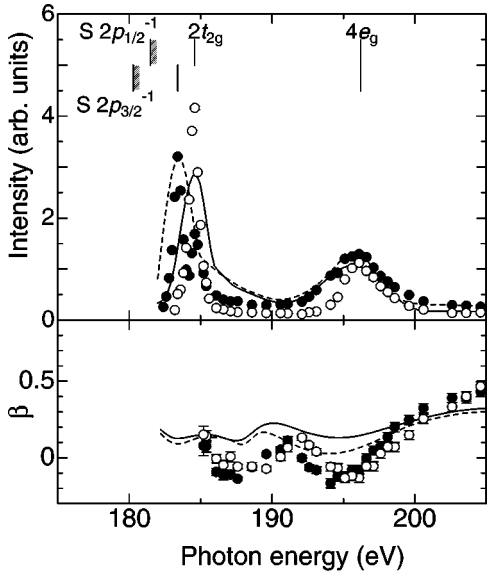

FIG. 2. (a) Relative partial photoionization cross sections of SF_6 into the $(S\ 2p_{3/2})^{-1}$ state (●) and the $(S\ 2p_{1/2})^{-1}$ state (○). Results of the CMS calculations for the $(S\ 2p_{3/2})^{-1}$ state (– – –) and the $(S\ 2p_{1/2})^{-1}$ state (——) are plotted together. CMS results are normalized to the experimental results at 196 eV. (b) Asymmetry parameter β for the S $2p$ photoelectrons from the photoionization into the $(S\ 2p_{3/2})^{-1}$ state (●) and the $(S\ 2p_{1/2})^{-1}$ state (○) with CMS calculations for the $(S\ 2p_{3/2})^{-1}$ state (– – –) and the $(S\ 2p_{1/2})^{-1}$ state (——).

of the incident photon. The S $2p$ photoelectron spectra were recorded at $\theta=0°$ and 90° as a function of photon energies and obtained relative partial cross sections σ and asymmetry parameters β. The degree of polarization P of the incident photon and the detection efficiency of the analyzer as a function of the angle were estimated by measuring the angular dependence of the $1s$ photoelectron of He and the $2s$ and $2p$ photoelectrons of Ne, whose angular distributions are well known. Total photoion yield spectra were also measured with the same apparatus by collecting almost all of the nonenergetic photoions using the stray field of the entrance lens of the analyzer and a high pass energy.

Photon energy bandwidth was ~200 meV for both the total photoion yield measurements and the energy and angular resolved photoelectron measurements, depending on the photon energies. Overall energy resolution and angular resolution in photoelectron measurements were ~0.4 eV and 10°, respectively. Possible systematic errors were estimated to be less than 10% for σ and ±0.1 for β.

The total photoion yield spectrum of SF_6 is shown in Fig. 1. The double-peaked structure of the $(S\ 2p_{3/2,1/2})^{-1}\ 6a_{1g}$ states is clearly seen at ~173 eV, below the S $2p$ ionization threshold. The double-peaked feature accounts for the splitting of final states by the spin-orbit interaction of the sulfur $2p$ electrons. Weak fine structures observed at 176 – 180 eV are one-electron excitations into Rydberg states. The most intense double-peaked structure at ~184 eV is the $(S\ 2p_{3/2,1/2})^{-1}\ 2t_{2g}$ resonance. Spin-orbit splitting between $(S\ 2p_{3/2})^{-1}\ 2t_{2g}$ and $(S\ 2p_{1/2})^{-1}\ 2t_{2g}$ of this resonance is about 1.1 eV, which is almost the same as the splitting of the S $2p$ ionization threshold. The broad peak at ~196 eV is assigned to the $(S\ 2p_{3/2,1/2})^{-1}\ 4e_g$ resonance. The broadening of the $(S\ 2p_{3/2,1/2})^{-1}\ 4e_g$ resonance may be due to the short lifetime of this resonance. Because of this broadening, the spin-orbit splitting of this resonance is not clear, in contrast to the former two peaks. All of these features resemble the high-resolution photoabsorption measurements of Hudson *et al.* [8]. It should be noted that a statistical model for the inner-shell-excited states would predict a doublet with a peak intensity ratio $(S\ 2p_{3/2})^{-1}$:$(S\ 2p_{1/2})^{-1}$ to be 2:1. The observed intensity ratios $(S\ 2p_{3/2})^{-1}\ 6a_{1g}$:$(S\ p_{1/2})^{-1}\ 6a_{1g}$ and $(S\ 2p_{3/2})^{-1}\ 2t_{2g}$:$(S\ 2p_{1/2})^{-1}\ 2t_{2g}$ are, however, both less than unity. This reversal of the intensity ratios has been explained by including the effects of the exchange interaction between the $(S\ 2p)^{-1}$ inner-shell hole and the excited electron (see, for example, Ref. [8], and references therein).

Figure 2 shows the relative partial photoionization cross sections $\sigma_{3/2}$ and $\sigma_{1/2}$ of SF_6 into the $(S\ 2p_{3/2})^{-1}$ and $(S\ 2p_{1/2})^{-1}$ states, respectively, together with the asymmetry parameters β of the S $2p$ photoelectrons. Both of the $(S\ 2p_{3/2,1/2})^{-1}\ 2t_{2g}$ and $(S\ 2p_{3/2,1/2})^{-1}\ 4e_g$ resonances are clearly seen for $\sigma_{3/2}$ and $\sigma_{1/2}$. Enhancement of $\sigma_{3/2}$ is observed not only at the $(S\ 2p_{3/2})^{-1}\ 2t_{2g}$ resonance, but also at the $(S\ 2p_{1/2})^{-1}\ 2t_{2g}$ resonance. It should be noted that the jj coupling approximation predicts no intensity of $\sigma_{3/2}$ at the $(S\ 2p_{1/2})^{-1}\ 2t_{2g}$ resonance. When the exchange interaction between the $(S\ 2p)^{-1}$ inner-shell hole and the t_{2g} electron is as significant as the spin-orbit interaction, the jj coupling approximation is no longer valid and thus the ''$(S\ 2p_{3/2})^{-1}\ 2t_{2g}$'' resonance ends by possessing not only the character of the $(S\ 2p_{3/2})^{-1}$ ionic core, but also the character of the $(S\ 2p_{1/2})^{-1}$ ionic core. As a result, the ionization into the $(S\ 2p_{1/2})^{-1}$ state becomes possible even at the ''$(S\ 2p_{3/2})^{-1}\ 2t_{2g}$'' resonance.

An enlargement of Fig. 2(a) around the $(S\ 2p_{3/2,1/2})^{-1}\ 2t_{2g}$ resonance region is shown in Fig. 3. No obvious evi-

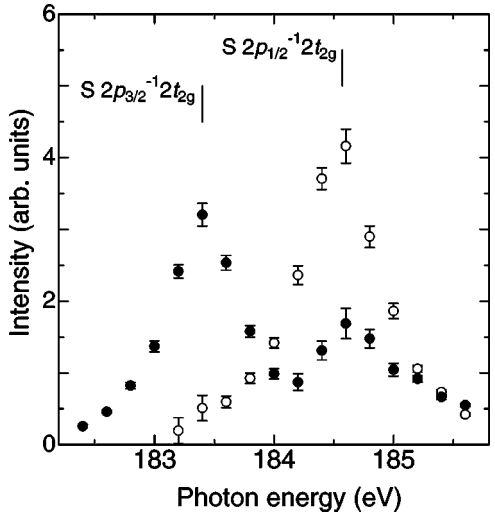

FIG. 3. Relative partial photoionization cross sections of SF_6 into the $(S\ 2p_{3/2})^{-1}$ state (●) and the $(S\ 2p_{1/2})^{-1}$ state (○) around the $(S\ 2p_{3/2,1/2})^{-1}\ t_{2g}$ resonances.

dence for the enhancement of $\sigma_{1/2}$ at the $(S\ 2p_{3/2})^{-1}\ 2t_{2g}$ resonance is observed. Since the energy for the $(S\ 2p_{3/2})^{-1}\ 2t_{2g}$ resonance is nearly at the threshold of the $(S\ 2p_{1/2})^{-1}$ state, postcollision interaction (PCI) effects may play a role in this observation. In the present photoion yield spectrum of Fig. 1, the peak widths of 0.68 eV and 0.72 eV are obtained by the Lorentzian fitting for the $(S\ 2p_{3/2})^{-1}\ 2t_{2g}$ resonance and the $(S\ 2p_{1/2})^{-1}\ 2t_{2g}$ resonance, respectively. Hudson *et al.* also found that the width of the $(S\ 2p_{1/2})^{-1}\ 2t_{2g}$ resonance peak is about 13% larger than that of the $(S\ 2p_{3/2})^{-1}\ 2t_{2g}$ resonance peak in their photoabsorption spectrum: they attributed this difference to the faster decay of the $(S\ 2p_{1/2})^{-1}$ inner-shell hole compared to the $(S\ 2p_{3/2})^{-1}$ inner-shell hole [8]. The faster decay of the $(S\ 2p_{1/2})^{-1}\ 2t_{2g}$ resonance might be explained by the present observation that the $(S\ 2p_{1/2})^{-1}\ 2t_{2g}$ resonance has a decay channel into the $(S\ 2p_{3/2})^{-1}$ state, while the $(S\ 2p_{3/2})^{-1}\ 2t_{2g}$ resonance does not decay into the $(S\ 2p_{1/2})^{-1}$ state. The ratio of the area of the $\sigma_{3/2}$ curve and that of the $\sigma_{1/2}$ curve at the $(S\ 2p_{3/2,1/2})^{-1}\ 2t_{2g}$ resonance region is 1.1:1, showing the breakdown of the pure jj coupling model in this region.

In the photon energy region between the $(S\ 2p_{3/2,1/2})^{-1}\ 2t_{2g}$ resonance and the $(S\ 2p_{3/2,1/2})^{-1}\ 4e_g$ resonance, both $\sigma_{3/2}$ and $\sigma_{1/2}$ remain almost constant. The intensity ratio between $\sigma_{3/2}$ and $\sigma_{1/2}$ is about 2:1, in agreement with the ratio predicted by the statistical model.

An interesting feature of $\sigma_{3/2}$ and $\sigma_{1/2}$ is observed at the $(S\ 2p_{3/2,1/2})^{-1}\ 4e_g$ resonance. Both the energy and the intensity at the maximum of the peak do not change between $\sigma_{3/2}$ and $\sigma_{1/2}$, while the peak width of $\sigma_{3/2}$ is larger than that of $\sigma_{1/2}$. The difference between $\sigma_{3/2}$ and $\sigma_{1/2}$ is noticeable at 190–195 eV, i.e., the lower energy side of the $(S\ 2p_{3/2,1/2})^{-1}\ 4e_g$ resonance. The ratio of the area of the $\sigma_{3/2}$ curve and that of the $\sigma_{1/2}$ curve at the $(S\ 2p_{3/2,1/2})^{-1}\ 4e_g$ resonance is 1.5:1, which is smaller than the value 2:1 expected by the statistical model. The smaller ratio than expected may also be due to the exchange interaction between the $(S\ 2p)^{-1}$ inner-shell hole and the $4e_g$ electron. The *ab initio* calculation of Francis *et al.*, in which the spin-orbit interactions were neglected, showed that the exchange interaction at the $(S\ 2p_{3/2,1/2})^{-1}\ 4e_g$ resonances is much stronger than that at the $(S\ 2p_{3/2,1/2})^{-1}\ t_{2g}$ resonances [9].

The photon energy dependence of the asymmetry parameter β plotted in Fig. 2(b) generally shows a decreasing feature from 0 to -0.1 with an increase in the photon energy from the threshold to 187 eV and an increasing feature toward 0.5 with an increase in the photon energy up to 210 eV, with a broad dip at about the $4e_g$ resonance. This general feature has been seen also in the measurement of Ferrett *et al.* [5]. A broad dip observed at slightly lower photon energy of the $(S\ 2p_{3/2,1/2})^{-1}\ 4e_g$ resonance has also been reported by Ferrett *et al.* [5]. The position of the dip of $\beta_{3/2}$ is lower than that of $\beta_{1/2}$ by 1.1 eV, i.e., the same amount as the spin-orbit splitting of the $(S\ 2p)^{-1}$ states.

Partial photoionization cross sections into the $(S\ 2p_{3/2})^{-1}$ state and the $(S\ 2p_{1/2})^{-1}$ state have also been calculated in the present study using the continuum multiple scattering (CMS) method, originally formulated by Dill and Dehmer [15]. The CMS method has been widely applied to electron-molecule scattering and has provided essential information on electron-molecule collisions [16]. This calculation reproduces well the resonance based on the shape resonance model. Only the spin-orbit interaction is accounted for in the present CMS calculation. The CMS results are also plotted together in Fig. 2.

Energies for the $(S\ 2p_{3/2,1/2})^{-1}\ 2t_{2g}$ resonance and the $(S\ 2p_{3/2,1/2})^{-1}\ 4e_g$ resonance are also well reproduced in the CMS calculation. The CMS calculation showed that the energy difference of the $(S\ 2p_{3/2})^{-1}\ 4e_g$ resonance and the $(S\ 2p_{1/2})^{-1}\ 4e_g$ resonance is much smaller than that of the spin-orbit splitting between the $(S\ 2p_{3/2})^{-1}$ state and the $(S\ 2p_{1/2})^{-1}$ state. The CMS partial cross-section curves, however, do not reproduce the spin-orbit state dependence observed in the experiment. Enhancement of the $\sigma_{3/2}$ at the $(S\ 2p_{1/2})^{-1}\ 2t_{2g}$ resonance is not reproduced due to the neglect of the exchange interaction in the present calculation. Relativistic calculations, which take account of both the spin-orbit interaction and the exchange interaction properly, may be necessary to obtain the observed spin-orbit state dependence correctly.

The general feature of the photon energy dependence of the asymmetry parameter β obtained by the CMS calculation agrees well with that of the experiment. The broad dip near the $(S\ 2p_{3/2,1/2})^{-1}\ 4e_g$ resonance is, however, much more enhanced in the experimental results than in the CMS result. In addition, the CMS results showed somewhat smaller $\beta_{3/2}$ than for $\beta_{1/2}$ in the whole energy region, although the experimental results showed that the $\beta_{3/2}$ and $\beta_{1/2}$ are essentially the same.

In the simple shape resonance model, the potential barrier is produced by the combination of the Coulomb attractive potential and the centrifugal barrier of the angular momentum of the outgoing photoelectron. The photoelectrons from the S $2p$ orbital will dominantly have *s*- and/or *d*-wave character. Near the S $2p$ ionization threshold, the *d*-wave has to

tunnel through a thick potential barrier caused by the angular momentum itself. Thus, the *s* wave dominates near the threshold region and, hence, $\beta=0$ is expected. The *d* wave ''feels'' a thinner potential barrier with increasing photon energy, and when the photon energy exceeds the ridge of the potential barrier, the *d* wave ''feels'' no potential barrier and thus a positive value of β is expected. Interference between the *s* wave and the *d* wave may cause a negative or positive additive to the β value and, hence, structures.

In conclusion, the angular distribution measurement of S $2p_{3/2}$ and S $2p_{1/2}$ photoelectrons in the photoionization of SF_6 in the vicinity of the shape resonances has been presented. The relative partial photoionization cross sections into the $(S\ 2p_{3/2})^{-1}$ state showed a clear enhancement not only at the $(S\ 2p_{3/2})^{-1}\ 2t_{2g}$ resonance, but also at the $(S\ 2p_{1/2})^{-1}\ 2t_{2g}$ resonance, indicating the exchange interaction between the $(S\ 2p)^{-1}$ inner-shell hole and the $2t_{2g}$ electron. At the $(S\ 2p_{3/2,1/2})^{-1}\ 4e_g$ resonance, both the energy and the intensity at the maximum of the photoionization cross sections peak did not differ between the $(S\ 2p_{3/2})^{-1}$ state and the $(S\ 2p_{1/2})^{-1}$ state, while the peak width of the $(S\ 2p_{3/2})^{-1}$ state was larger than that of the $(S\ 2p_{1/2})^{-1}$ state. Kinetic-energy dependences of the asymmetry parameter β of the S $2p_{3/2}$ and S $2p_{1/2}$ photoelectrons, $\beta_{3/2}$ and $\beta_{1/2}$, respectively, showed no clear spin-orbit state dependence. Continuum multiple-scattering (CMS) calculation of the asymmetry parameters for the $(S\ 2p_{3/2})^{-1}$ and $(S\ 2p_{1/2})^{-1}$ states reproduced this behavior. The shape of β curves results from the changing of the Coulomb phase-shift differences between the *s*-like and *d*-like outgoing photoelectrons. However, the present experimental and CMS results showed that the contribution from the molecular resonance to the β curve was small.

This experiment was carried out with the approval of the Photon Factory Advisory Committee (Proposal No. 97G302) and partly supported by Grant-in-aid for Scientific Research from the Japanese Ministry of Education, Science, Sports, and Culture and by the Matsuo Foundation.

[1] R. E. LaVilla and R. D. Deslattes, J. Chem. Phys. **44**, 4399 (1966).
[2] T. M. Zimkina and V. A. Fomichev, Sov. Phys. Dokl. **11**, 726 (1967).
[3] A. S. Vinogradov and T. M. Zimkina, Opt. Spectrosc. **31**, 364 (1971).
[4] A. P. Hitchock and C. E. Brion, Chem. Phys. **33**, 55 (1978).
[5] T. A. Ferrett, D. W. Lindle, P. A. Heimann, M. N. Piancastelli, P. H. Kobrin, H. G. Kerkhoff, U. Becker, W. D. Brewer, and D. A. Shirley, J. Chem. Phys. **89**, 4726 (1988).
[6] B. M. Addison-Jones, K. H. Tan, B. W. Yates, J. N. Cutler, G. M. Bancroft, and J. S. Tse, J. Electron Spectrosc. Relat. Phenom. **48**, 155 (1989).
[7] J. S. Tse and Z. F. Liu, Phys. Rev. A **44**, 7838 (1991).
[8] E. Hudson, D. A. Shirley, M. Domke, G. Remmers, A. Puschmann, T. Mandel, C. Xue, and G. Kaindl, Phys. Rev. A **47**, 361 (1993).
[9] J. T. Francis, C. C. Turci, T. Tyliszczak, G. G. de Souza, N. Kosugi, and A. P. Hitchcock, Phys. Rev. A **52**, 4665 (1995).
[10] K. Ueda, Y. Shimizu, H. Chiba, M. Okunishi, K. Ohmori, J. B. West, Y. Sato, T. Hayaishi, H. Nakamatsu, and T. Mukoyama, Phys. Rev. Lett. **79**, 3371 (1997).
[11] J. L. Dehmer, J. Chem. Phys. **56**, 4496 (1972).
[12] H. Nakamatsu, T. Mukoyama, and H. Adachi, J. Chem. Phys. **95**, 3167 (1991).
[13] A. Yagishita, T. Hayaishi, T. Kikuchi, and E. Shigemasa, Nucl. Instrum. Methods Phys. Res. A **306**, 578 (1991).
[14] Y. Shimizu, K. Nagao, K. Ueda, M. Takahashi, H. Chiba, S. Yanagida, M. Okunishi, K. Ohmori, Y. Sato, T. Hayaishi, and K. J. Ross, J. Electron Spectrosc. Relat. Phenom. **88-91**, 1031 (1998).
[15] D. Dill and J. L. Dehmer, J. Chem. Phys. **61**, 692 (1974).
[16] M. Kimura and H. Sato, Comments At. Mol. Phys. **26**, 333 (1991).